

1-Bit SubTHz RIS with Planar Tightly Coupled Dipoles: Beam Shaping and Prototypes

Xianjun Ma*, Yonggang Zhou*, Qi Luo[†], Yihan Ma[†], Kyriakos Stylianopoulos[‡], and George C. Alexandropoulos[‡]

* Nanjing University of Aeronautics and Astronautics, Nanjing, China

[†] University of Hertfordshire, Hatfield, UK

[‡] Department of Informatics and Telecommunications, National and Kapodistrian University of Athens, Greece
emails: zyg405@nuaa.edu.cn, {q.luo2, y.ma20}@herts.ac.uk, {kstylianop, alexandg}@di.uoa.gr

Abstract—In this paper, a proof-of-concept study of a 1-bit wideband reconfigurable intelligent surface (RIS) comprising planar tightly coupled dipoles (PTCD) is presented. The developed RIS operates at subTHz frequencies and a 3-dB gain bandwidth of 27.4% with the center frequency at 102 GHz is shown to be obtainable via full-wave electromagnetic simulations. The binary phase shift offered by each RIS unit element is enabled by changing the polarization of the reflected wave by 180°. The proposed PTCD-based RIS has a planar configuration with one dielectric layer bonded to a ground plane, and hence, it can be fabricated by using cost-effective printed circuit board (PCB) technology. We analytically calculate the response of the entire designed RIS and showcase that a good agreement between that result and equivalent full-wave simulations is obtained. To efficiently compute the 1-bit RIS response for different pointing directions, thus, designing a directive beam codebook, we devise a fast approximate beamforming optimization approach, which is compared with time-consuming full-wave simulations. Finally, to prove our concept, we present several passive prototypes with frozen beams for the proposed 1-bit wideband RIS.

Index Terms—Reconfigurable intelligent surface, tightly coupled dipole, THz, beam shaping, wideband.

I. INTRODUCTION

Reconfigurable intelligent surfaces (RISs) have been identified as one of the key physical layer technologies for the upcoming sixth generation (6G) of wireless communications [1], [2], [3]. Such metasurfaces are capable of reflecting their incident waves to desired angles, enriching specular channels with scattering, and enabling over-the-air analogue computations [4], [5], paving the way for the envisioned smart wireless environments [6], [7]. Another highly expected feature of 6G is the promising utilization of the THz frequency band that encapsulates extensive unallocated bandwidth, which can be used to support rate- and localization/sensing-demanding applications, while exhibiting increased confidentiality and anti-interference capabilities [8].

The combination of the latter two 6G technologies is lately attracting significant research [9], [10], mainly due to the fact that reconfigurable metasurfaces can contribute in extending the coverage of THz links. RIS unit cells operating at THz were recently presented in [11], [12], [13], where the tunable characteristics of their reflective beams were achieved through a tunable dielectric substrate equipped with voltage control. In [14], the beam tuning characteristics were dynamically

controlled based on a liquid crystal unit structure, indicating that this design method of reconfigurable reflection arrays is a promising one for THz RISs. A broadband tightly coupled reflectarray structure has been also reported for THz RIS unit elements in [15], [16]. According to the relevant literature, the tightly coupled dipole technology has the advantage of being ultra wideband for antenna application, which makes tightly coupled antenna elements another candidate design solution for THz RISs. In fact, remarkable progress has been made in the design of tightly coupled RIS unit elements for those frequencies, and 1-bit and 2-bit wideband and ultra-wideband reflectarrays have been designed [17], [18], [19].

In this paper, we capitalize on our recent ultra-wideband subTHz RIS [20], which was based on tightly coupled dipoles that are vertically placed on a ground plane, and present a novel efficient RIS unit element design. Although the elements in the design of [20] can be fabricated by using conventional printed circuit board (PCB) technology, the assembly of each individual RIS element is challenging and the mechanical robustness of the overall design is poor. We have thus improved that design by modifying the RIS unit cell to a planar structure. This design can be easily fabricated via multi-layer PCB technology with significantly reduced complexity and cost for the assembly process. Compared with the design in [20], the bandwidth of the presented subTHz RIS design is reduced, but the resulting planar tightly coupled dipoles (PTCD)-based RIS still possesses a wideband response. In particular, the simulated 3-dB gain bandwidth is 27.4% with the center frequency at 102 GHz.

The remainder of the paper is organized as follows. Section II details the design of the proposed RIS unit cell, including full-wave simulations for the entire RIS. Section III presents the beamforming modeling and algorithmic approach to calculate the response of the developed 1-bit wideband RIS to arbitrary directions, while Section IV concludes the paper.

II. THE PROPOSED PTCD-BASED SUBTHZ RIS DESIGN

In this section, we present the configuration of the planar tightly coupled dipole, which is used as the unit element of the proposed subTHz RIS. Simulated radiation patterns via electromagnetic (EM) software of the entire RIS are also included and discussed.

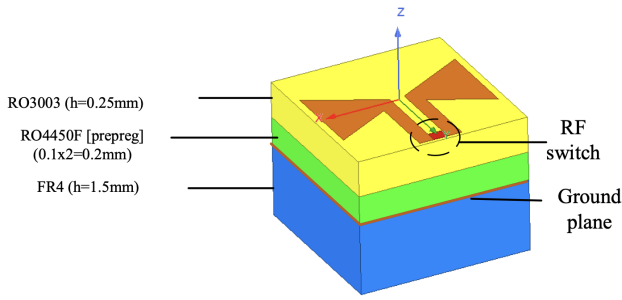


Fig. 1. The illustration in 3D of the designed RIS unit cell, which is a planar tightly coupled butterfly dipole printed on the top layers of the substrate. The RIS element is linearly polarized in the x -axis. An RF switch is placed in the middle of the dipole to rotate the polarization of the impinging wave.

A. 1-Bit Unit Cell Design

Fig. 1 illustrates the configuration of the proposed PTC structure which constitutes the unit cell of the designed sub-THz RIS. The unit cell is designed with a printed butterfly dipole element placed on a RO3003 substrate with a thickness of 0.25 mm. Below the RO3003, there is a RO4450F substrate with a thickness of 0.2 mm, which is also backed by a ground plane on the other side. Additionally, another dielectric layer, FR4 with a thickness of 1.5 mm, is introduced below the metallic ground to enhance the overall structure's mechanical strength. As a result, the total thickness of the reflecting unit cell is 2 mm, including the thickness of the copper layers. By controlling the ON/OFF states of the RF switch placed at the same layer of the printed dipole, the reflection phase of the unit cell can be tuned with 180° phase difference. As a proof-of-concept study, at this stage, we model the RF switch as an ideal one and do not consider the equivalent circuit model of the switch, which is left for the extension of this work.

The current distribution of the dipole for different states of the RF switch is depicted in Figs. 2 and 3. As shown, the surface current on the planar dipole was rotated by 180° , implying that the polarization of the reflected wave is changed by 180° . In this simulation, a linear polarized normal incident wave along the x direction is employed to illuminate the dipole antenna with the same linear polarization. Figs. 4 and 5 demonstrate the corresponding reflection phase and amplitude of the unit cell with binary phase states, considering the normal incident angle. As shown in Fig. 4, the RIS unit cell shows low insertion loss. It is noted that the actual insertion loss of the RIS unit cell will be higher when considering the equivalent circuit model of the subTHz switch. From Fig. 5, it can be seen that the unit cell exhibits a wideband phase response with stable 180° phase differences from the frequency 88 to 116 GHz for the two different states of the RF switch.

B. RIS Design and Simulated Response

We use the previously presented unit cell to synthesize an RIS aperture comprising 31×31 elements in CST Microwave Studio. Considering the limitation of the testing facility, we choose to place the source of the incident wave relatively close

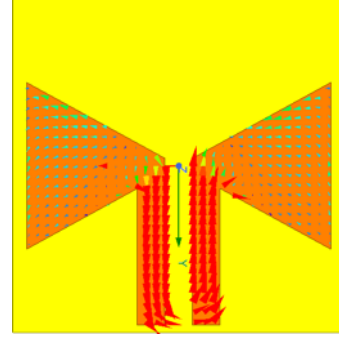


Fig. 2. The current distribution of the designed 1-bit RIS unit cell when the RF switch is ON.

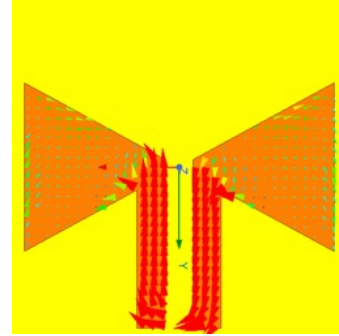


Fig. 3. The current distribution of the designed 1-bit RIS unit cell when the RF switch is OFF.

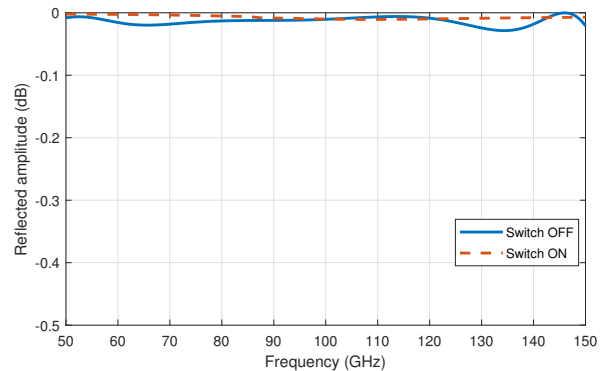


Fig. 4. The reflection amplitude of the designed 1-bit RIS unit cell when the RF switch is ON and OFF as a function of the operating frequency in the $[88.5, 116.7]$ GHz range.

to the RIS, and in particular, we set $f/D = 0.5$, where f is the focal distance and D is the diameter of the aperture of the reflecting surface. The simulation model for the designed RIS is illustrated in Fig. 6.

In Fig. 7, the simulated radiation pattern of the designed RIS at the H -plane is demonstrated when the reflection beam is configured to 22.5° . It is noted that despite the phase error resulting from the 1-bit phase quantization, the beam pointing error is small and the sidelobe level (SLL) is larger than 10 dB. We have also conducted full-wave EM simulations to extract the active radiation pattern of the unit cell and

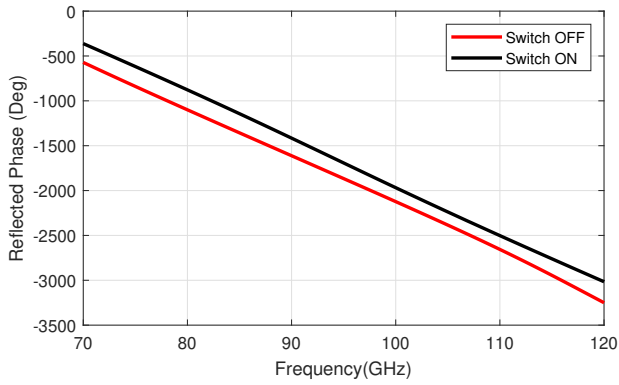


Fig. 5. The reflection phase of the designed 1-bit RIS unit cell when the RF switch is ON and OFF as a function of the operating frequency in the [88.5, 116.7] GHz range.

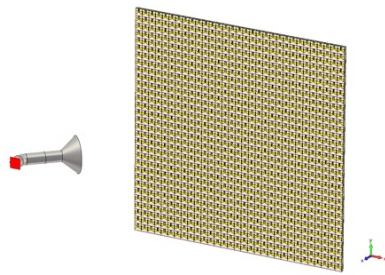


Fig. 6. The simulation model of the wideband subTHz RIS consisting of 31×31 tightly-coupled dipole elements.

analytically calculated the response of the entire RIS. Figs. 10 and 11 depict the results of the pattern calculated by the active method and that of equivalent EM simulations, when the RIS is reconfigured to 0° and 22.5° beam scanning, respectively. The approximated beams will be discussed next in Section III. As observed, the analytical results agree well with the simulated results for the main beam, while some differences are present in the SLLs. The disagreement is mainly caused due to the fact that, during the analytical calculation, we ignored the change of the mutual couplings at the edge elements and the response of the RIS unit cell with arbitrary incident angles. According to the simulation results, it was found that when the RIS reflects the incident wave to foresight, the 3-dB gain bandwidth is 27.4% with the center frequency at 102 GHz.

To validate the proposed wideband subTHz RIS design with 1-bit PTC-based unit cells and evaluate the fabrication accuracy, several passive prototypes have been fabricated. These prototypes were designed to provide reflection beams pointing at the fixed angles 0° , 22.5° , and 45° . Fig. 8 shows a photo of one of the fabricated prototypes. Fig. 9 shows the comparison between the measured and simulated radiation pattern with the beam steered to 22.5° degree. As shown, good agreement at the main lobe is obtained.

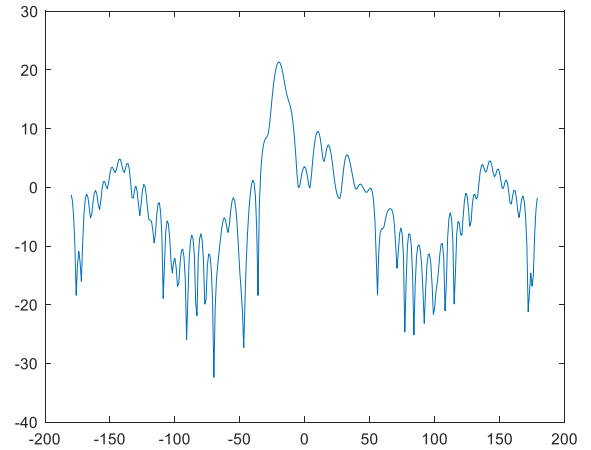


Fig. 7. The simulated radiation of the designed wideband subTHz RIS when the beam is configured to point to the 22.5° direction.

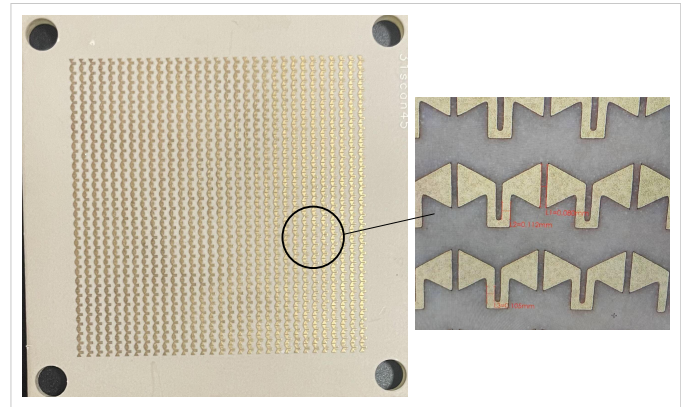


Fig. 8. Photo of the fabricated 31×31 subTHz RIS with 1-bit unit cells.

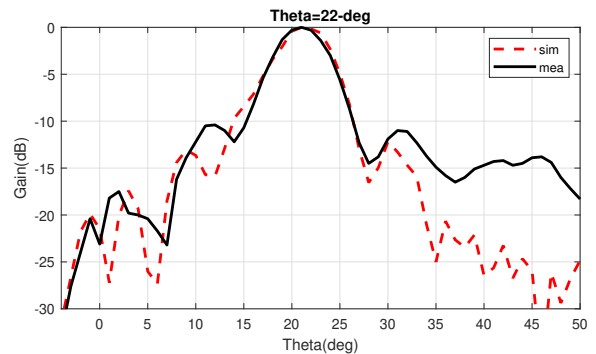


Fig. 9. The measured and simulated radiation of the designed wideband subTHz RIS when the beam is configured to point to the 22.5° direction.

III. RIS BEAM SHAPING OPTIMIZATION

In this section, we capitalize on the RIS beamforming optimization approach recently developed in [21] to devise reflection beams for the proposed wideband PTC-based 1-bit RIS design to any desired direction. This approach can

be quite efficient for efficiently designing static as well as dynamic RIS beam codebooks for communications [22], [23], [24], localization/sensing [10], [25], as well integrated sensing and communications [26].

To deploy the approach in [21], we consider a system model comprising a single-antenna transmitter (TX) placed in front of the center of the broadside of the designed RIS as in Section II-B, and a candidate receiver (RX) antenna at an intended position \mathbf{p} . Considering the pure line of sight (LoS) reflected link from the TX to the RX, and given an arbitrary RIS configuration vector $\boldsymbol{\omega}^T \in \mathbb{C}^{M \times 1}$ for an RIS of M unit cells, the corresponding beam pattern toward \mathbf{p} has the form:

$$G(\mathbf{p}) = \boldsymbol{\omega}^T \mathbf{b}(\mathbf{p}, \mathbf{p}_{\text{TX}}), \quad (1)$$

where $\boldsymbol{\omega}$ is an M -element column vector including the RIS beam pattern and T represents vector transposition, \mathbf{p}_{TX} is the TX position, $\mathbf{b}(\mathbf{p}, \mathbf{p}_{\text{TX}}) = \mathbf{a}(\mathbf{p}) \odot \mathbf{a}(\mathbf{p}_{\text{TX}})$, with \odot denoting the element-wise product, and $[\mathbf{a}(\mathbf{p})]_m = \exp(-j\frac{2\pi}{\lambda}(\|\mathbf{p} - \mathbf{p}_m\| - \|\mathbf{p} - \mathbf{p}_{\text{RIS}}\|))$ denotes the beam-focusing vector with λ being the wavelength, \mathbf{p}_m is the position of the m -th ($m = 1, 2, \dots, M$) RIS unit cell, and \mathbf{p}_{RIS} represents the RIS center location. This formulation holds both for near- and far-field scenarios, however, for our specific setup, we choose the RX coordinates at a fixed distance well beyond the Fraunhofer limit to investigate beam patterns that depend only on the targeted RX's angles. The positions of the TX, \mathbf{p}_{TX} , and that of the RIS, \mathbf{p}_{RIS} , are considered fixed. According to [21, Sec. 3.2], the RIS beam pattern $\boldsymbol{\omega}$ in (1) can be optimized to realize any desired reflection beam for any given RX position, disregarding the environmental factors of path loss, transmission power, and RX noise. To this end, the beam pattern for a directional beam can be represented by:

$$G(\mathbf{p}) = (\mathbf{b}^*(\mathbf{p}, \mathbf{p}_{\text{TX}}))^T \mathbf{b}(\mathbf{p}, \mathbf{p}_{\text{TX}}), \quad (2)$$

where $\mathbf{b}^*(\mathbf{p}, \mathbf{p}_{\text{TX}}) = \boldsymbol{\omega}^T$ is the conjugate of $\mathbf{b}(\mathbf{p}, \mathbf{p}_{\text{TX}})$.

Following this system modeling approach, the obtained phase shifts of the RIS configuration fall under the continuous regime in $[0, 2\pi]$. Then, using the derivations presented in [21], a discretized beam pattern $\hat{G}(\mathbf{p})$ (i.e., a discrete approximation of $G(\mathbf{p})$) can be numerically computed, whose states are guaranteed to belong in an arbitrary discrete set \mathcal{K} . For the 1-bit subTHz RIS design presented in the previous Section II-B, the phase shift of each RIS unit cell can take values from the discrete set $\mathcal{K} = \{0, \pi\}$, while their reflection amplitudes can be safely assumed to be unitary. The RIS beam-shaping methodology involves iteratively taking appropriately scaled gradient steps over a modified version of the unconstrained objective, before projecting onto the feasible set of solutions. The complete formulation and algorithmic approach for RIS beam shaping is given in Algorithm 3 of [21].

In the previously discussed Figs. 10 and 11, patterns for the approximated beams designed using [21]'s Algorithm 3 are included, and compared with equivalent analytically computed ones as well as beam patterns obtained by full-wave EM simulations of the fabricated unit cells. As it can be seen, the gain of each beam pattern is normalized in the dB scale,

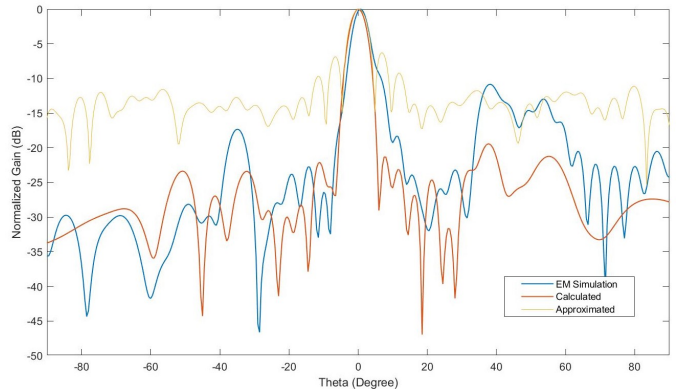


Fig. 10. Full-wave EM simulated, analytical, and approximated beam patterns when the RIS is configured to reflect the incident wave to the 0° direction.

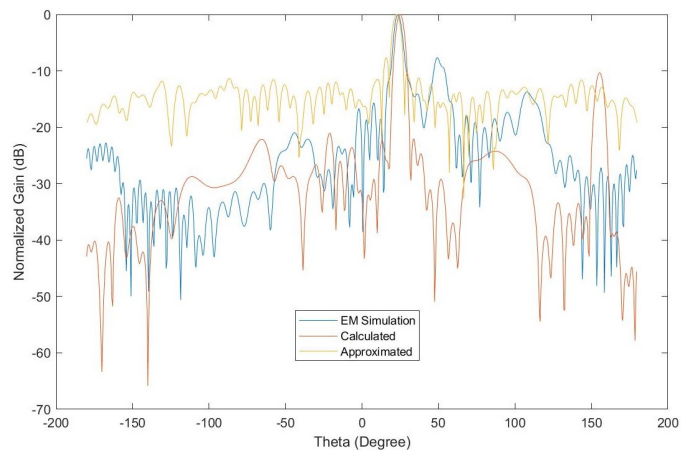


Fig. 11. Full-wave EM simulated, analytical, and approximated beam patterns when the RIS is configured to reflect the incident wave to the 22.5° direction.

i.e., the main lobe's gain is 0 dB. It can be observed that the approximated beam patterns can achieve effective focusing at the desired pointing angles since the beam widths at these angles almost coincide among all three cases. The SLL levels of the approximated beams are between 6.5 and 7 dB, and the overall beam profiles are flatter and with SLLs placed more closely to the main lobe, as compared to full-wave EM simulations and theoretical calculations for the fabricated responses. All in all, the results in these two figures indicate that, while arbitrary discrete configurations can be produced to perform beam steering at desired angles, more accurate approximation approaches and algorithms are required to reduce reflections at the SLLs. In future work, we plan to extend the approach in [21] to consider tunable tradeoffs between the gains of the main lobe and those of the SLLs.

IV. CONCLUSION

A wideband RIS design operating at the subTHz frequency band was presented in this paper. The proposed design comprised PTC-based unit cells, each being integrated with an RF switch for realizing a 1-bit phase shift. The conducted full-wave EM simulations showcased that the designed RIS has

excellent beam scanning ability. Directional beams in different direction angles were realized by modifying the 1-bit phase distribution of the RIS structure.

To deal with the increased complexity of extremely large RIS/array full-wave EM simulations, we presented a fast approximate beam shaping approach that, based on a projection gradient descent technique, approximates ideal continuous reflection patterns to obtain beam patterns of arbitrary large realistic RISs with unit cells of effectively discrete phase shifts. It was demonstrated that the proposed beam shaping approximation technique exhibits sufficient agreement with equivalent full-wave EM simulations in the main lobes while requiring further refinement to match the SLL behavior. The latter constitutes our future research direction which will pave the way for efficient designs of static as well as dynamic beam codebooks for extremely large RIS in subTHz and THz bands.

ACKNOWLEDGMENTS

This work was supported by the UK Royal Society with grant number IESR2 212064 and the Smart Networks and Services Joint Undertaking (SNS JU) under the European Union's Horizon Europe research and innovation programme under Grant Agreement No 101097101, including top-up funding by UK Research and Innovation (UKRI) under the UK government's Horizon Europe funding guarantee.

REFERENCES

- [1] "Reconfigurable intelligent surfaces (RIS): Use cases, deployment scenarios and requirements," ETSI GR RIS 001, ETSI, Apr. 2023.
- [2] G. C. Alexandropoulos, G. Lerosey, M. Debbah, and M. Fink, "Reconfigurable intelligent surfaces and metamaterials: The potential of wave propagation control for 6G wireless communications," *IEEE ComSoc TCCN Newsl.*, vol. 6, no. 1, pp. 25–37, Jun. 2020.
- [3] M. Jian, G. C. Alexandropoulos, E. Basar, C. Huang, R. Liu, Y. Liu, and C. Yuen, "Reconfigurable intelligent surfaces for wireless communications: Overview of hardware designs, channel models, and estimation techniques," *Intell. Converged Netw.*, vol. 3, no. 1, pp. 1–32, Mar. 2022.
- [4] Q. Li, M. Wen, S. Wang, G. C. Alexandropoulos, and Y.-C. Wu, "Space shift keying with reconfigurable intelligent surfaces: Phase configuration designs and performance analysis," *IEEE Open J. Commun. Society*, vol. 2, pp. 322–333, Feb. 2021.
- [5] G. C. Alexandropoulos, N. Shlezinger, and P. del Hougne, "Reconfigurable intelligent surfaces for rich scattering wireless communications: Recent experiments, challenges, and opportunities," *IEEE Commun. Mag.*, vol. 59, no. 6, pp. 28–34, Jun. 2021.
- [6] E. Calvanese Strinati, G. C. Alexandropoulos, H. Wymeersch, B. Denis, V. Sciancalepore, R. D'Errico, A. Clemente, D.-T. Phan-Huy, E. De Carvalho, and P. Popovski, "Reconfigurable, intelligent, and sustainable wireless environments for 6G smart connectivity," *IEEE Commun. Mag.*, vol. 59, no. 10, pp. 99–105, Oct. 2021.
- [7] G. C. Alexandropoulos, D.-T. Phan-Huy, K. D. Katsanos, M. Crozzoli, H. Wymeersch, P. Popovski, P. Ratajczak, Y. Bénédict, M.-H. Hamon, S. Herraiz Gonzalez, P. Mursia, M. Rossanese, V. Sciancalepore, J.-B. Gros, S. Terranova, G. Gradoni, P. Di Lorenzo, M. Rahal, B. Denis, R. D'Errico, A. Clemente, and E. Calvanese Strinati, "RIS-enabled smart wireless environments: Deployment scenarios, network architecture, bandwidth and area of influence," *EURASIP J. Wireless Commun. Netw.*, to appear, 2023.
- [8] C. Han, Y. Wang, Y. Li, Y. Chen, N. A. Abbasi, T. Kürner, and A. F. Molisch, "Terahertz wireless channels: A holistic survey on measurement, modeling, and analysis," *IEEE Communications Surveys & Tutorials*, vol. 24, no. 3, pp. 1670–1707, 2022.
- [9] "TERahertz ReconfigurAble METAsurfaces for ultra-high rate wireless communications (TERRAMETA) SNS JU Project," <https://terrameta-project.eu/>.
- [10] K. Keykhosravi, B. Denis, G. C. Alexandropoulos, Z. S. He, A. Albanese, V. Sciancalepore, and H. Wymeersch, "Leveraging RIS-enabled smart signal propagation for solving infeasible localization problems," *IEEE Veh. Technol. Mag.*, vol. 18, no. 2, pp. 20–28, Jun. 2023.
- [11] B. A. Çelebi, I. Aras, K. E. Özçelik, K. Tekbiyik, G. Kurt, O. Özdemir, and A. R. Ekti, "Accurate modelling of reconfigurable intelligent surfaces in THz band," in *Proc. 29th Signal Process. Commun. Appl. Conf.*, Istanbul, Turkey, Jun. 2021.
- [12] K. Rasilainen, T. D. Phan, M. Berg, A. Pärssinen, and P. J. Soh, "Hardware aspects of Sub-THz antennas and reconfigurable intelligent surfaces for 6G communications," *IEEE J. Sel. Areas Commun.*, vol. 41, no. 8, pp. 2530–2546, Aug. 2023.
- [13] S. Saab, S. A. Surra, G. Xu, and R. W. Heath, "An inverted L-shaped multi-layer reconfigurable intelligent surface for THz communications," in *Proc. Asilomar Conf. Signals, Sys., Comp.*, Pacific Grove, USA, Jun. 2022.
- [14] D. Jun, Y. Youn, C. Lee, M. Hwang, W. Hong, and C. B. Chae, "Real-time implementation of semi-active reconfigurable intelligent surfaces for mmWave and Sub-THz systems," in *Proc. IEEE Consumer Commun. Netw. Conf.*, Las Vegas, USA, Jan. 2023.
- [15] W. Li, H. Tu, Y. He, L. Zhang, S.-W. Wong, and S. Gao, "A novel wideband tightly coupled dual-polarized reflectarray antenna," *IEEE Trans. Antennas Propag.*, vol. 71, no. 6, pp. 5422–5427, Jun. 2023.
- [16] J. Wang, Y. Zhou, S. Gao, and Q. Luo, "An efficiency-improved tightly coupled dipole reflectarray antenna using variant-coupling-capacitance method," *IEEE Access*, vol. 8, pp. 37 314–37 320, Feb. 2020.
- [17] H. Kamoda, T. Iwasaki, J. Tsumochi, T. Kuki, and O. Hashimoto, "60-GHz electronically reconfigurable large reflectarray using single-bit phase shifters," *IEEE Trans. Antennas Prop.*, vol. 59, no. 7, pp. 2524–2531, Jul. 2011.
- [18] J. Han, L. Li, G. Liu, Z. Wu, and Y. Shi, "A wideband 1 bit 12×12 reconfigurable beam-scanning reflectarray: Design, fabrication, and measurement," *IEEE Antennas Wireless Propag. Lett.*, vol. 18, no. 6, pp. 1268–1272, Jun. 2019.
- [19] Q. Luo, S. Gao, W. Li, X. Yang, and G. Wen, "Ultra-wideband and multiband reflectarrays for intelligent multi-functional platforms," in *Proc. European Conf. Antennas Propag.*, Krakow, Poland, Mar. 2019, pp. 1–5.
- [20] Q. Luo, G. C. Alexandropoulos, Y. Zhou, and X. Ma, "Ultra-wideband metasurface at SubTHz: Hardware design and reflection optimization," in *Proc. European Conf. Antennas Propag.*, Florence, Italy, Mar. 2020, pp. 1–5.
- [21] M. Rahal, B. Denis, K. Keykhosravi, M. F. Keskin, B. Uguen, G. C. Alexandropoulos, and H. Wymeersch, "Performance of RIS-aided nearfield localization under beams approximation from real hardware characterization," *EURASIP J. Wireless Commun. Netw.*, to appear, 2023.
- [22] V. Jamali, G. C. Alexandropoulos, R. Schober, and H. V. Poor, "Low-to-zero-overhead IRS reconfiguration: Decoupling illumination and channel estimation," *IEEE Commun. Lett.*, vol. 16, no. 4, pp. 932–936, Apr. 2022.
- [23] G. C. Alexandropoulos, V. Jamali, R. Schober, and H. V. Poor, "Near-field hierarchical beam management for RIS-enabled millimeter wave multi-antenna systems," in *Proc. Sensor Array Multich. Signal Process. Works.*, Trondheim, Norway, Jun. 2022.
- [24] J. An, C. Xu, Q. Wu, D. W. K. Ng, M. Di Renzo, C. Yuen, and L. Hanzo, "Codebook-based solutions for reconfigurable intelligent surfaces and their open challenges," *IEEE Wireless Commun.*, to appear, 2023.
- [25] G. C. Alexandropoulos, I. Vinieratou, and H. Wymeersch, "Localization via multiple reconfigurable intelligent surfaces equipped with single receive RF chains," *IEEE Wireless Commun. Lett.*, vol. 11, no. 5, pp. 1072–1076, May 2022.
- [26] S. P. Chepuri, N. Shlezinger, F. Liu, G. C. Alexandropoulos, S. Buzzi, and Y. C. Eldar, "Integrated sensing and communications with reconfigurable intelligent surfaces," *IEEE Signal Process. Mag.*, vol. 40, no. 6, pp. 41–62, Sep. 2023.